New insights into diagnostic values and mechanisms of ferroptosis associated with immune infiltration in diabetic kidney disease

YING TAN[1], ZIHUI LIU[2], SIYUAN SONG[2], LINGLING ZHU[2], YUN SHE[2], XIQIAO ZHOU[1], JIANGYI YU[1] and QIANHUA YAN[1]

[1]Department of Endocrinology, Jiangsu Hospital of Chinese Medicine, Nanjing, Jiangsu 210029, P.R. China; [2]The First Clinical Medical College, Nanjing University of Chinese Medicine, Nanjing, Jiangsu 210023, P.R. China

Received October 7, 2025; Accepted July 7, 2026

DOI: 10.3892/etm.2026.13278

Abstract. The pathogenesis of diabetic kidney disease (DKD) is complex and closely related to ferroptosis and immune dysregulation, but the relevance is unclear. The present study investigates the potential mechanisms of ferroptosis-related genes (FRGs) in DKD and their relationship with the immune-inflammatory response. It searches for new diagnostic biomarkers to help diagnose and treat DKD. Four Gene Expression Omnibus (GEO) datasets, GSE30528, GSE30529 and GSE30122 as the test set, and GSE96804 for validation, were analyzed. FRGs were obtained from GeneCards, and 47 ferroptosis-related differentially expressed genes (FRDEGs) were identified by intersecting with DKD-related differentially expressed genes. Functional enrichment analyses, including Gene Ontology, Kyoto Encyclopedia of Genes and Genomes, Gene Set Enrichment Analysis and Gene Set Variation Analysis, revealed that these FRDEGs are primarily associated with ferroptosis, hypoxia response and immune inflammation. Subsequently, the weighted gene co-expression network analysis (WGCNA) was employed to expand the ferroptosis-related gene network, and intersection of the 47 FRDEGs with key WGCNA module genes yielded 10 key genes. Based on the 10 key genes, the least absolute shrinkage and selection operator and support vector machine algorithms identified three hub genes [chemokine ligand 5 (CCL5), forkhead box C1 (FOXC1) and lactotransferrin (LTF)] for DKD diagnosis. Receiver operating characteristic curves confirmed their diagnostic value, with FOXC1 and LTF validated in the independent dataset. Immune infiltration analysis via CIBERSORT revealed eight immune cell types with significantly different infiltration levels between the DKD and control group in the integrated GEO datasets. Notably, both LTF and CCL5 showed a significant positive correlation with gamma delta T cells (γδT). Quantitative PCR results confirmed differential expression of the three hub genes in the DKD group, with elevated expression observed in DKD mice following intervention with rosiglitazone and hyperoside.

Correspondence to: Professor Qianhua Yan or Professor Jiangyi Yu, Department of Endocrinology, Jiangsu Hospital of Chinese Medicine, 155 Hanzhong Road, Qinhuai, Nanjing, Jiangsu 210029, P.R. China
E-mail: yanqianhua@njucm.edu.cn
E-mail: yjy202105@njucm.edu.cn

Key words: diabetic kidney disease, ferroptosis, bioinformatics analysis, diagnostic biomarkers, immune infiltration

Introduction

Diabetic kidney disease (DKD) is one of the most serious microvascular complications of diabetes mellitus, with its incidence steadily rising and has become the primary cause of end-stage kidney disease (ESKD) in Europe, the United States, and Asian countries (1,2). Despite the evidence from several randomized controlled trials demonstrating the efficacy of renin-angiotensin system inhibitors, sodium-glucose cotransporter 2 inhibitors, and non-steroidal mineralocorticoid receptor antagonists in reducing renal endpoints, there remains a persistent risk of DKD progression. The incidence of DKD and resulting ESKD is still on the rise, and the available Western medical treatments have not yet led to an inflection point in the occurrence and progression of DKD. Once DKD has progressed to severe renal insufficiency, it is considered an irreversible and extremely high-risk stage; therefore, there is a pressing need to continually investigate more sensitive biomarkers for the diagnosis and intervention of DKD.

Ferroptosis, a form of iron-dependent cell death driven by lipid peroxidation discovered in 2012, is caused by an imbalance in cellular redox homeostasis, leading to massive lipid peroxidation and eventual accumulation of excess iron-dependent lipid hydroperoxides to lethal levels, which in turn causes intracellular mitochondrial atrophy, an increase in the density of bilayers, and a decrease in or disappearance of the mitochondrial cristae (3). It is widely investigated in the fields of oncology, heart failure and neurological diseases (4). Since the presence of ferroptosis in DKD was first reported in 2020 (5), a growing amount of research evidence suggests that ferroptosis is an essential driver in the development of DKD, which can damage a wide range of renal intrinsic cells and reduce renal function (6). Additionally, inhibition of ferroptosis can effectively delay the development of renal lesions in diabetic mice (4). The pathogenesis of DKD is complex

and involves multiple pathways, such as metabolic disorders, hemodynamic abnormalities, inflammation and fibrosis reactions, oxidative stress and cell death (7). However, the exact mechanism remains unclear. Previous studies have primarily focused on metabolic and hemodynamic changes (8), but increasing evidence suggests that immune disorders and inflammatory responses play a crucial role in the occurrence and progression of DKD (9). Recently, it has also been shown that ferroptosis can trigger kidney injury through an immune cell-mediated inflammatory response (10), and monitoring the degree of kidney immune infiltration and inflammation may guide clinical decision-making. However, the mechanisms underlying abnormal iron metabolism and immune inflammation in DKD remain unclear.

In the present study, bioinformatics technology was used to screen differentially expressed genes (DEGs) associated with ferroptosis in DKD and reveal the biological functions and signal transduction pathways they are involved in, as well as to obtain key genes by combining WGCNA. Hub genes were obtained based on key genes to construct and validate the DKD diagnostic model. The correlation between hub genes and immune infiltration was also explored. The results of the present study would help provide new ideas for the pathogenesis of DKD and new molecular targets for the treatment of DKD.

Materials and methods

Microarray dataset collection and data process. The DKD-related datasets GSE30528 (11), GSE30529 (11), GSE30122 (11,12) and GSE96804 (13,14) were downloaded from the GEO database via the R package GEOquery (15), in which the datasets GSE30528, GSE30529 and GSE30122 served as the test set and the dataset GSE96804 served as the validation set. All DKD samples and control samples were included in the present study. The characteristics of these datasets are listed in Table SI. The R package sva (16) was used to de-batch the datasets GSE30528, GSE30529 and GSE30122 to obtain the combined GEO datasets, which contained 19 DKD samples and 50 control samples. Finally, the combined GEO datasets and dataset GSE96804 were subjected to normalization using the R package limma (17), along with annotation of probes and other standardization and normalization procedures.

Ferroptosis-related genes (FRGs) were collected from the GeneCards database by searching for 'ferroptosis' and retaining only those categorized as 'Protein Coding', yielding 654 FRGs (18). Additionally, a systematic literature search on PubMed using the keyword 'ferroptosis' was performed, and FRGs with at least one *in vitro* or *in vivo* experimental validation reported in peer-reviewed publications were manually curated, yielding 60 FRGs (19). After merging and removing duplicates, a final set of 667 FRGs was obtained (Table SII). The data processing flowchart is depicted in Fig. 1.

Ferroptosis-related differentially expressed genes (FRDEGs) screening. The R package limma (17) was utilized to analyze the gene expression differences between the DKD and control samples. A threshold of |logFC|>0.0 and adj. P<0.05 was established to identify DEGs, with the intent of maximizing the capture of FRGs exhibiting statistically significant changes in DKD. This initial screening strategy was subsequently complemented by multi-step stringent filtering to ensure the robustness of the final diagnostic biomarkers. Specifically, genes with logFC >0.0 and adj. P<0.05 were considered upregulated, while genes with logFC <0.0 and adj. P<0.05 were deemed downregulated. Subsequently, the DEGs were intersected with FRGs to obtain FRDEGs. The R package ggplot2 demonstrated the results of the differential analysis for volcano mapping.

Gene set enrichment and variation analysis. To determine the effect of expression levels of all genes in the combined GEO datasets on DKD, gene set enrichment analysis (GSEA) (20) and gene set variation analysis (GSVA) (21) were performed to explore the differences in pathways and biological processes of the samples in the combined GEO datasets. The c2.all.v7.5.1.symbols.gmt gene set for GSEA and GSVA was obtained from the Molecular Signatures Database (MSigDB) database (22). The screening criteria for GSEA were adj. P<0.05 and FDR value (q-value) <0.25, and the screening criteria for GSVA were |logFC|>0.50 and P<0.05.

Gene ontology (GO) and kyoto encyclopedia of genes and genomes (KEGG) enrichment analysis. GO analysis (23) is essential for exploring biological function, including biological process (BP), cellular component (CC) and molecular function (MF). The KEGG (24) is a widely used database storing information about genomes, biological pathways diseases and drugs and is often used to explore potential pathways. GO and KEGG analysis of FRDEGs were performed using the R package clusterProfiler (25), with screening criteria of adj. P<0.05 and FDR value (q-value) <0.25 considered statistically significant, and adj.p correction by Benjamini-Hochberg.

Weighted gene co-expression network analysis (WGCNA). In order to screen the co-expression modules of the combined GEO datasets and analyze the core genes in the network, WGCNA was performed on the genes in the top 25% of the variance of all samples in the combined GEO datasets using the R package WGCNA package (26). During the process, the correlation of both DKD and control groups with different modules was measured, and the genes in each module were recorded, where the genes in each module were considered module signature genes. Finally, the modules with |r value| >0.30 were screened, and all the genes in the modules were intersected with FRDEGs respectively. All the intersected genes obtained from the different modules were the key genes.

Construction and verification of the DKD diagnostic model. In order to obtain the DKD diagnostic model of combined GEO datasets, the key genes were screened with P<0.05. Subsequently, a logistic regression model was constructed, and the molecular expression of the key genes included in this model was illustrated using a Forest Plot. Furthermore, Least Absolute Shrinkage and Selection Operator (LASSO) regression analysis was performed on the selected key genes included in the logistic regression model using the R package glmnet (27), with the parameter set.seed '500'. The outcomes of the LASSO regression analysis were visually

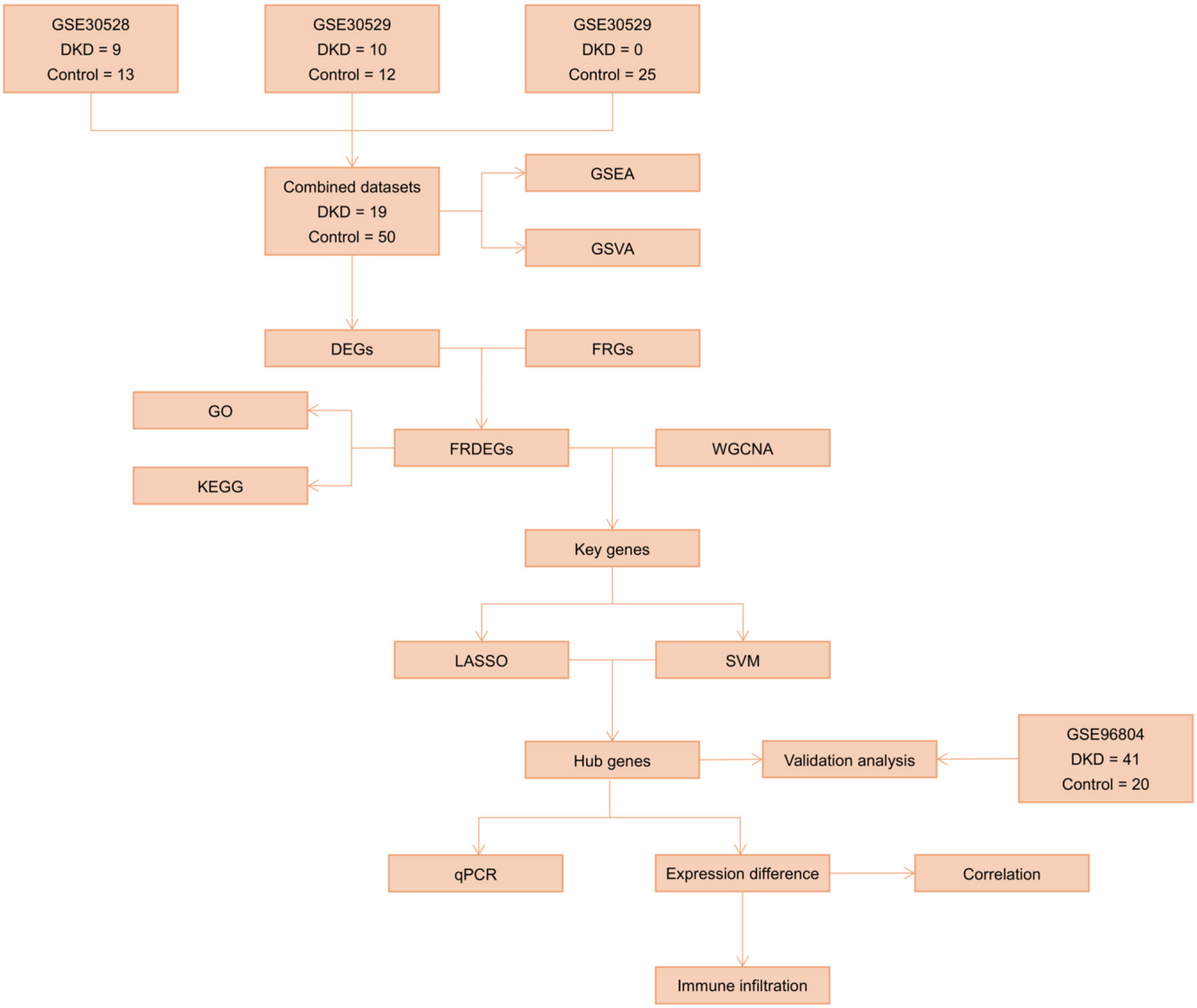

Figure 1. Flow chart for the comprehensive analysis of FRDEGs. DKD, diabetic kidney disease; DEGs, differentially expressed genes; FRGs, ferroptosis-related genes; GSEA, gene set enrichment analysis; GSVA, gene set variation analysis; GO, Gene Ontology; KEGG, Kyoto Encyclopedia of Genes and Genomes; FRDEGs, ferroptosis-related DEGs; WGCNA, weighted correlation network analysis; LASSO, least absolute shrinkage and selection operator; SVM, support vector machine; qPCR, quantitative polymerase chain reaction.

presented through diagnostic model plots and variable trajectory plots. In addition, the Support Vector Machine (SVM) model was constructed based on key genes by the SVM (28) algorithm and the key genes were screened based on the number of genes with the highest accuracy and lowest error rate. The key genes in the LASSO regression model and those in the SVM model were taken as intersections to get ferroptosis-related hub genes. R package rms drew a nomogram based on the results of LASSO regression analysis to show the interrelationships of ferroptosis-related hub genes.

To validate the accuracy and resolution of the DKD diagnostic model, the R package ggDCA was used to plot decision curve analysis (DCA) (29) based on the ferroptosis-related hub genes in the combined GEO datasets. Meanwhile, the R package pROC was used to plot the combined ROC curves in the combined GEO datasets and calculate the area under the curve (AUC) values to assess the diagnostic effect of LASSO risk score expression on the occurrence of DKD. The AUC of the ROC curves generally ranges between 0.5 and 1. The closer the AUC is to 1, the better the diagnostic effect. The AUC has a low accuracy at 0.5 to 0.7, a certain accuracy at 0.7 to 0.9, and a high accuracy at AUC above 0.9. The formula for calculating the LASSO risk score is as follows:

$$\text{riskScore} = \sum_{i} \text{Coefficient}\left(\text{gene}_i\right) \text{x mRNA Expression}\left(\text{gene}_i\right)$$

The dataset GSE96804 verified the accuracy and resolution of this DKD diagnostic model.

Identification and validation of the optimal Hub FRDEGs. Group comparisons were plotted based on the expression of ferroptosis-related hub genes in the DKD and control groups in the training and validation sets. R package pROC was used to plot the ROC curves of ferroptosis-related hub genes in the

training and validation sets and calculate the AUC to assess the diagnostic effect of the expression of ferroptosis-related hub genes on the occurrence of DKD.

Immune cell infiltration analysis. CIBERSORT (30) is based on the principle of linear support vector regression for the back-convolution of transcriptome expression matrices to estimate the composition and abundance of immune cells in a mixture of cells. The CIBERSORT algorithm was used to combine the LM22 feature gene matrix and filter the output of data with immune cell enrichment scores greater than zero to finally obtain the specific results of the immune cell infiltration matrix. Finally, the R package ggplot2 was used to draw group comparison plots to show the expression differences of LM22 immune cells in the DKD and control groups in the combined GEO datasets. The R package pheatmap was used to draw correlation heatmaps to show the LM22 immune cells and the correlation analysis results between ferroptosis-related hub genes and LM22 immune cells.

Reverse transcription-quantitative PCR (RT-qPCR). In the present study, a total of 9 male db/db mice (BKS. Cg-Leprdb/Leprdb) and 3 male db/m littermates (BKS. Cg-Leprdb/+) were obtained from Jiangsu Ailingfei Biotechnology Co., Ltd. db/m mice were used in the control group and db/db mice in the DKD group as the DKD model. All mice were 8 weeks of age at the start of the study, with body weights of 40±2.5 g for db/db mice and 25±2 g for db/m mice. The animals were housed in a specific pathogen-free facility under controlled conditions: Temperature, 23±2˚C; humidity, 50-60%; and a 12/12 h light/dark cycle, with free access to standard chow and water. Mice were acclimated for 1 week prior to the experiment. Both rosiglitazone (RZ) and hyperoside (HPS) groups used db/db mice as DKD models, and the two groups were gavaged respectively with RZ (cat. no. 210310; Chengdu Hengrui Pharmaceutical Co., Ltd.) at a dose of 5 mg/kg/d and HPS (cat. no. B20631; Shanghai Yuanye Biotechnology Co., Ltd.) at a quantity of 20 mg/kg/d. The intervention period was 12 weeks. Total RNA was extracted from the kidney of mice using the Animal Total RNA Isolation Kit (cat. no. RE-03011; Chengdu Fuji Biotechnology Co., Ltd.) and quantified using a spectrophotometer (cat. no. N50Touch; Implen GmbH). The thermocycling conditions for qPCR were as follows: Initial denaturation at 95˚C for 2 min, followed by 40 cycles of denaturation at 95˚C for 10 sec and annealing/extension at 60˚C for 30 sec. A melting curve analysis was performed from 65 to 95˚C with a ramp rate of 0.5˚C/5 sec. Relative quantification was performed using the comparative quantification cycle (Cq) ($2^{-\Delta\Delta Cq}$) method (31). The iScript™ cDNA Synthesis Kit (cat. no. 1708891; Bio-Rad Laboratories, Inc.) was used strictly according to the manufacturer's instructions. The standard reverse transcription temperature protocol includes primer annealing at 65˚C for 5 min followed by immediate ice incubation, cDNA synthesis at 42-55˚C for 20-60 min [42-45˚C for oligo(dT), 50-55˚C for thermostable reverse transcriptases and GC-rich RNA], and final enzyme inactivation at 70-85˚C for 5-15 min. Subsequently, qPCR was performed using the Sso Advanced™ Universal SYBR® Green Supermix kit (cat. no. 1725274; Bio-Rad Laboratories, Inc.) to detect the expression of lactotransferrin (LTF). The experiment was repeated at least three times with three sub-wells for each experiment. The primer sequences utilized in the investigation are presented in Table SIII. Anesthesia was performed when conducting animal sampling and surgical manipulation in the present study. Pentobarbital sodium as the anesthetic agent at a dosage of 50 mg/kg body weight, administered via intraperitoneal injection. All experimental mice were humanely euthanized by cervical dislocation after isoflurane inhalation anesthesia. Animal experiments were approved by the Animal Ethics Committee in Affiliated Hospital of Nanjing University of Traditional Chinese Medicine (approval no. 2023DW-039-01; Nanjing, China).

Statistical analysis. Data processing and analysis were based on R software (version 4.2.0) and GraphPad Prism (version 9.5.0; Dotmatics). The continuous variables were presented as the mean ± standard deviation. Comparisons between the two groups were made using the Wilcoxon rank sum test. If not specified, results were calculated by Spearman's correlation analysis of the correlation coefficients between the different molecules. $P<0.05$ was used as a criterion for statistically significant difference.

Results

Identification of FRDEGs. Firstly, the distribution box plots indicated the successful elimination of the batch effect in the DKD dataset following the batch removal procedure (Fig. 2A and B). Among the combined GEO datasets, 1,237 DEGs were identified, with 731 genes exhibiting upregulation and 506 genes displaying down-regulation (Fig. 2C). By intersecting the 1,237 DEGs with the 667 FRGs, a subset of 47 FRDEGs was obtained, which were LTF, CD44, CYBB, chemokine ligand 5 (CCL5), IGKC, RBBP4, ENO1, ALOX5, PRKCB, LCN2, TPM1, TUBA1A, PDIA4, CASP8, XRCC5, LASP1, ACTB, RPA2, HELLS, PTEN, SIAH2, ACSL4, GFRA1, KRT19, ANXA4, HNRNPL, EEF1A1, MUC1, CTNNB1, FHL2, PGK1, LPIN2, TP53, PDIA6, CP, CAD, VDAC1, SNAP29, SOX15, NFE2L1, G0S2, ALOX12, DLX2, CA9, CLTB, Forkhead box C1 (FOXC1) and TYRO3 (Fig. 2D). Then, based on the intersection results, the results of the expression differences of FRDEGs among different sample subgroups in the combined GEO datasets were shown in Fig. 2E.

GSEA and GSVA for the combined GEO datasets. To avoid the one-sidedness caused by only using the intersection gene enrichment, we also utilized GSEA on all the genes of the combined GEO datasets. The findings of the GSEA indicated that most genes exerted a significant impact on the inflammatory response pathway IL18 signaling pathway, IL-12 pathway and apoptosis, among others (Fig. 3A-E). The specific outcomes are presented in Table SIV.

The GSVA results showed that a total of 24 pathways exhibited statistical significance ($P<0.05$) in both the DKD and control groups (Fig. 4A and B). The DKD group exhibited a notable enrichment in the regulation of pathways associated with immunity, phosphorylation, apoptosis, methylation and deacetylation, such as the T cell receptor signaling pathway, monocyte signaling pathway, neutrophil signaling pathway, as well as the regulation of runt-related transcription factors

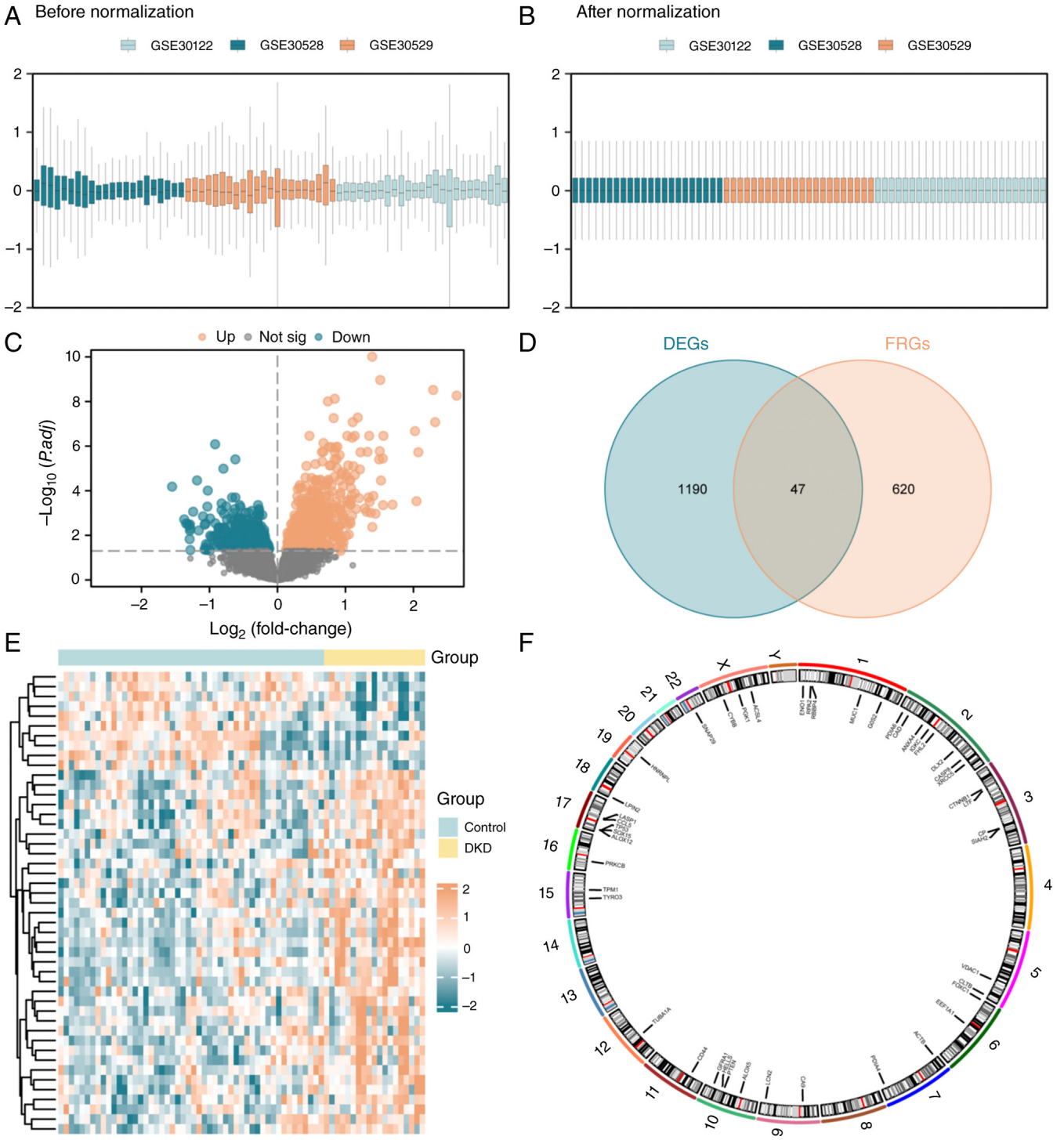

Figure 2. Batch effects removal and differential gene expression analysis. (A) Box line plots of the distribution of the combined GEO datasets before de-batch processing. (B) Box line plots of the distribution of the combined GEO datasets after de-batch processing. (C) Volcano plot of differentially expressed genes analyzed in the DKD and control groups in the combined GEO datasets. Blue nodes represent downregulation in DKD; orange nodes represent upregulation; and gray nodes represent no significant difference from controls. (D) The Venn diagram of differentially expressed genes and FRGs in the combined GEO datasets. (E) Correlation heatmap of ferroptosis-related differentially expressed genes in the combined GEO datasets. The control group shown in blue and the DKD group in yellow. (F) Chromosomal localization map of ferroptosis-related differentially expressed genes. DKD, diabetic kidney disease; DEGs, differentially expressed genes; FRGs, ferroptosis-related genes; FRDEGs, ferroptosis-related DEGs.

and histone deacetylases. Conversely, pathways linked to lipid synthesis and accumulation were found to be suppressed. The details can be found in Table SV.

Enrichment analysis of FRDEGs. A total of 47 FRDEGs were performed for enrichment analysis (Fig. 5A). In GO-BP analysis (Fig. 5B), the FRDEGs were mainly related to apoptosis regulation and cell proliferation. In GO-CC analysis (Fig. 5C), cell cortex, cell membrane and macromolecular compounds were significantly enriched. The results of enrichment analysis in GO-MF (Fig. 5D) indicated that these FRDEGs were mainly related to protein, enzyme and transcription factors.

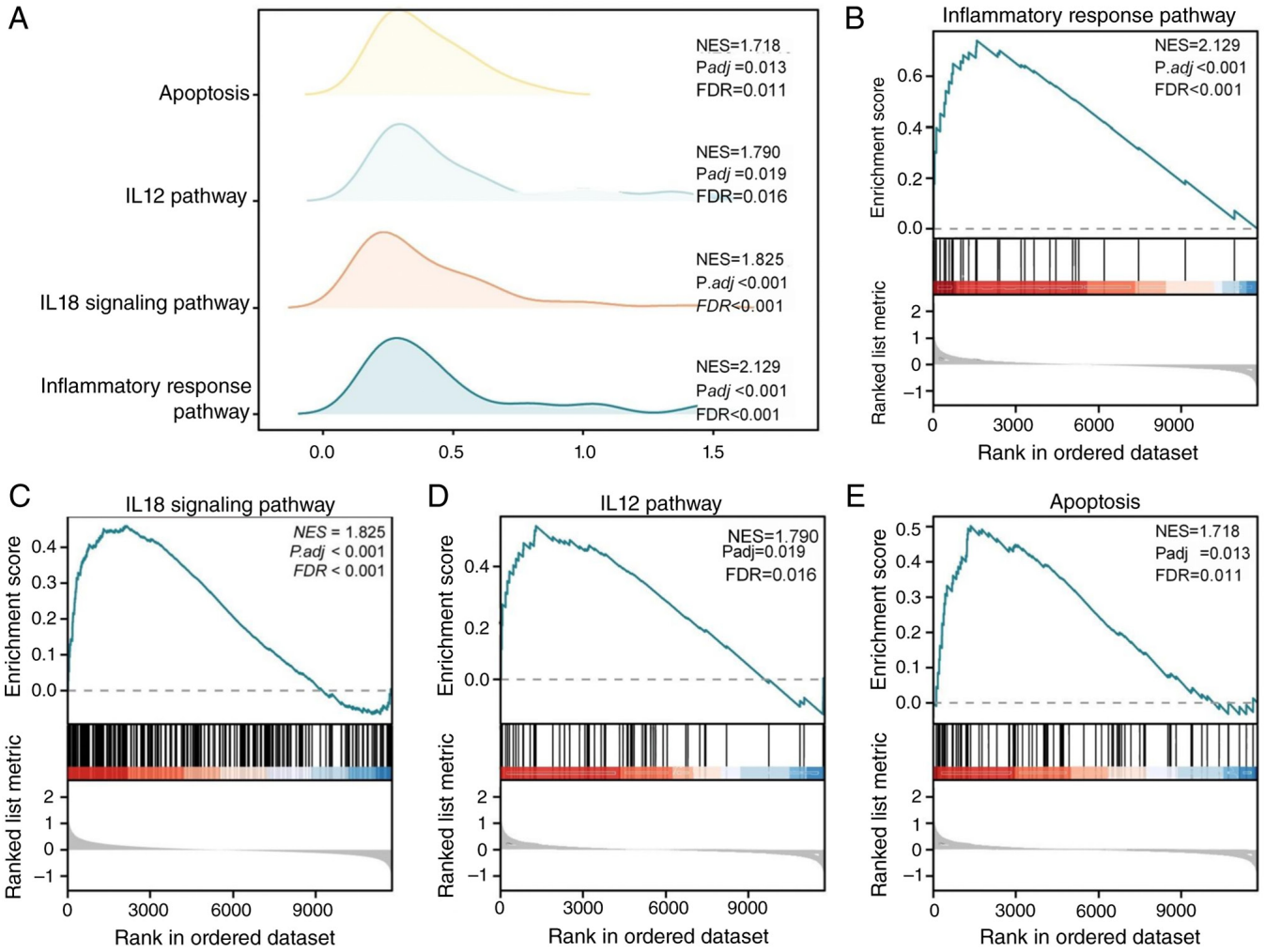

Figure 3. GSEA for combined GEO datasets. (A) The combined GEO datasets of the four biological functions of GSEA shown in a mountain range plot. (B) GSEA showed that DKD significantly affected inflammatory response pathway. (C) GSEA showed that DKD significantly affected the IL-18 signaling pathway. (D) GSEA showed that DKD significantly affected the IL-12 pathway. (E) GSEA showed that DKD significantly affected apoptosis. The GSEA screening criteria were adj. P<0.05 and FDR value (q-value) <0.25. GSEA, Gene Set Enrichment Analysis; GEO, Gene Expression Omnibus; DKD, diabetic kidney disease; FDR, false discovery rate.

According to the results of the KEGG analysis, these FRDEGs were mainly associated with ferroptosis, HIF-1 signaling pathway, leukocyte trans-endothelial migration and Influenza A (Fig. 5E).

Construction of co-expression modules and determination of key genes. Firstly, the constructed network exhibited higher conformity with the scale-free topology, as evidenced by the computation and presentation of scale-free fitting indices (Fig. 6A) across various soft threshold values. The findings indicated that a scale-free fitting index of 0.85 corresponds to the minimum soft threshold value of 11, which fulfilled the criteria for constructing an optimal scale-free network. The co-expression network was constructed using the optimal soft threshold, and genes with the top 25% variance are clustered using a clustering tree (Fig. 6B) and labeled with the grouping information. The results showed that genes in the top 25% of variance were clustered into 10 modules when the screening criterion was 0.2, and then the relationship between the genes and the merged modules was visualized (Fig. 6C). The correlation between all genes in the ten modules and the DKD group and control group in the combined GEO datasets was determined based on the expression patterns of the module genes (Fig. 6D). Genes within the MEyellow (|r value|=0.45) and MEblue (|r value|=0.32) modules were screened using a criterion of |r value|>0.30, and their intersections with the 47 FRDEGs were plotted using Venn diagrams (Fig. 6E and F). Ultimately, 10 key genes were identified: FOXC1, G0S2, TYRO3, CCL5, FHL2, IGKC, LCN2, LTF, MUC1 and PRKCB.

Construction and validation of the prognostic DKD model of FRGs. Logistic regression was performed based on the ten key genes, and a logistic regression model was constructed and visualized by Forest Plot (Fig. 7A). The results showed that all 10 key genes included in the logistic regression model were statistically significant (P<0.05). Then, the LASSO regression model (Fig. 7B and C) was constructed based on 10 key genes, and the results contained four key genes, which were CCL5, FOXC1, G0S2, and LTF. Meanwhile, the SVM model was constructed based on 10 key genes and the SVM algorithm to get the number of genes with the lowest error rate (Fig. 7D) and the highest accuracy (Fig. 7E). The results showed that the SVM model has

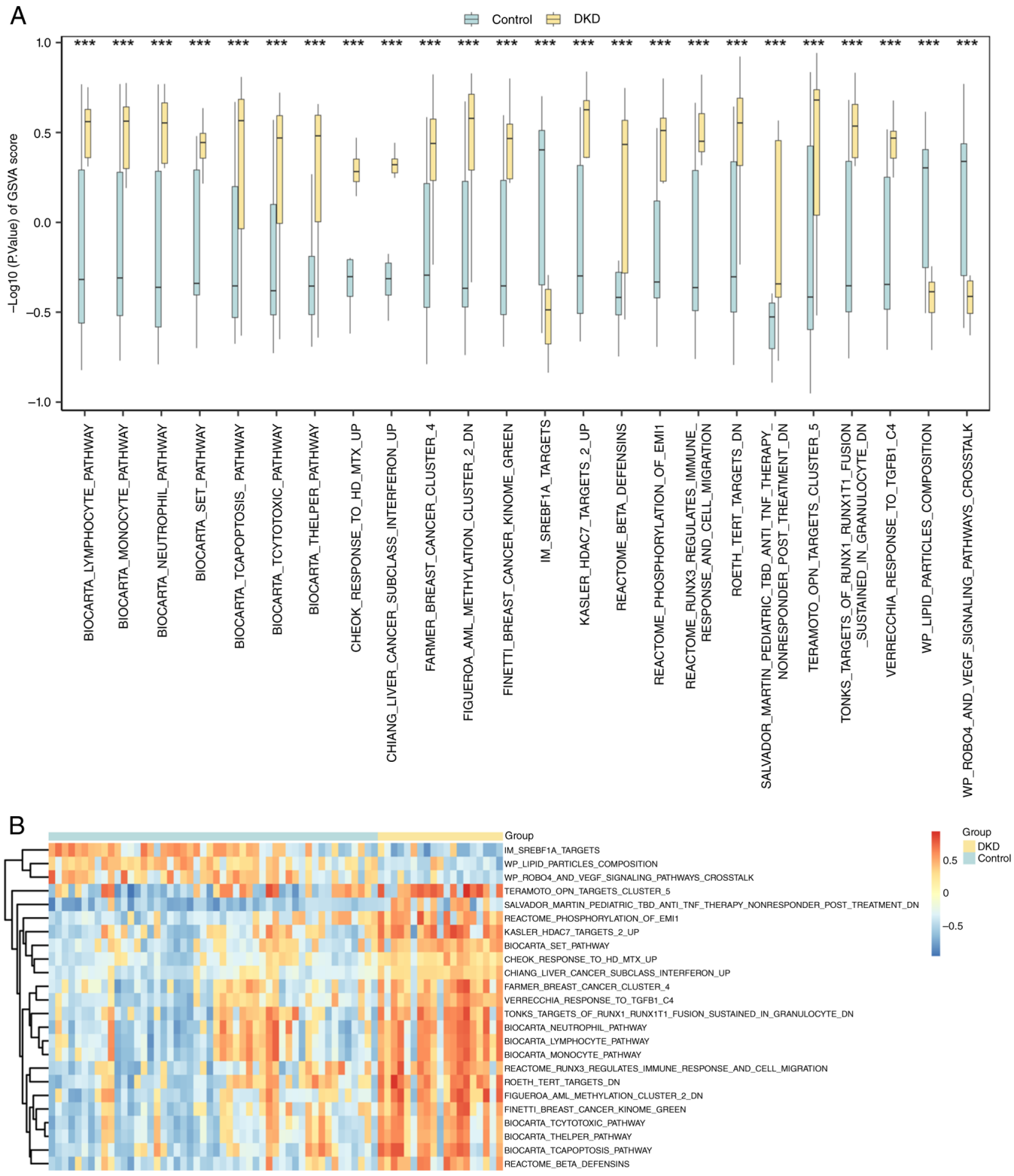

Figure 4. GSVA for combined GEO datasets. (A) Subgroup comparison box line plot of GSVA results between the DKD and control groups. (B) Complex value heat map of GSVA results between the DKD and control groups. The control group shown in blue and the DKD group shown in yellow. ***P<0.001. The screening criteria for GSVA were |log (fold change)|>0.50 and P<0.05. GSVA, gene set variation analysis; GEO, Gene Expression Omnibus; DKD, diabetic kidney disease.

the highest accuracy when the number of genes is 5. The five key genes were LTF, PRKCB, CCL5, MUC1 and FOXC1. The intersection of the key genes of the two models was received and three ferroptosis-related hub genes were obtained, CCL5, FOXC1 and LTF (Fig. 7F). Finally, to further validate the value of the DKD diagnostic model, a nomogram was developed to illustrate the interrelationships of ferroptosis-related hub genes, as depicted in Fig. 7G. The findings indicated that the expression of LTF exhibited notably greater efficacy in the DKD diagnostic model compared with other variables, while the expression of

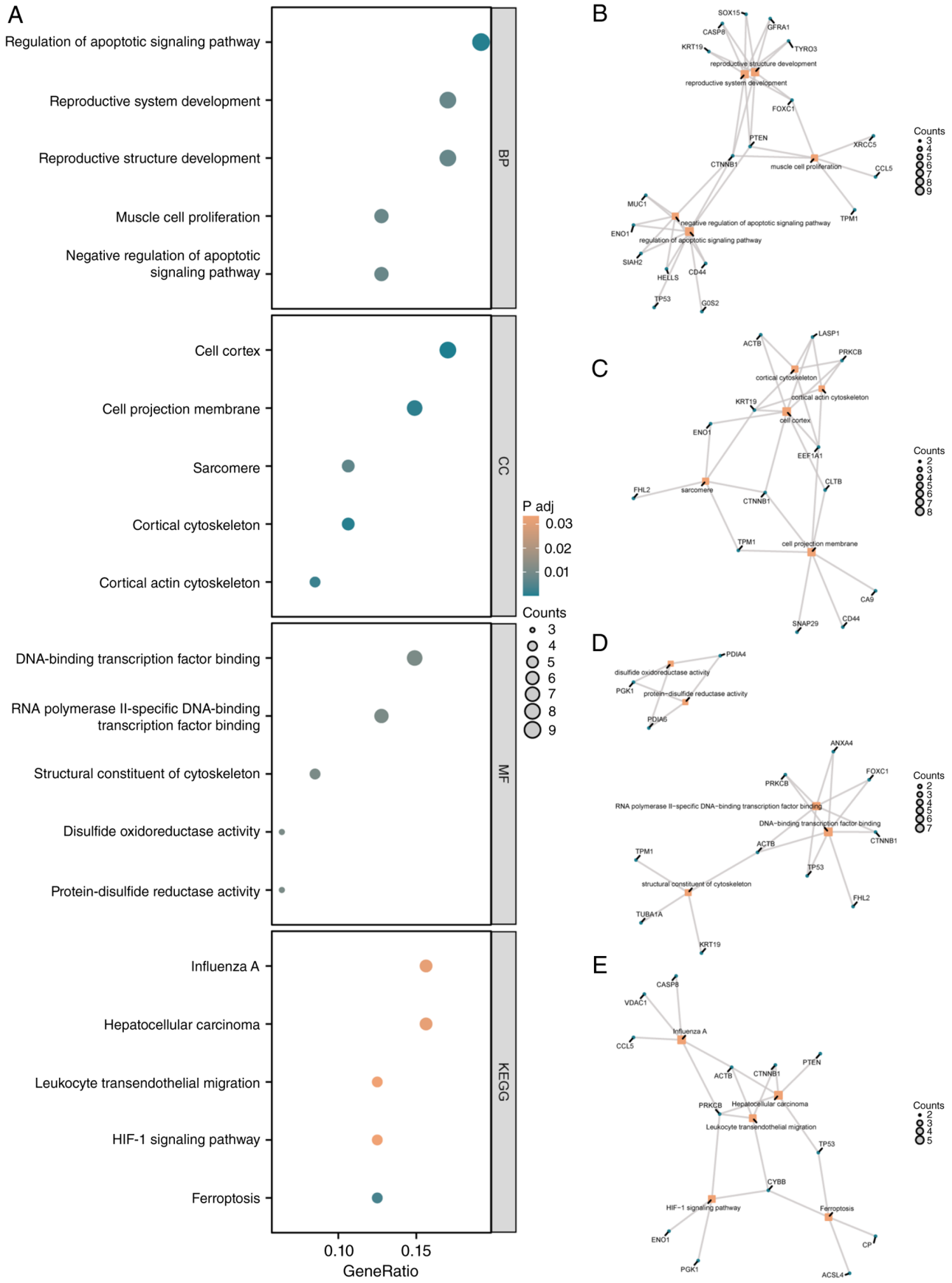

Figure 5. GO and KEGG enrichment analysis for FRDEGs. (A) Bubble plots showing the results of GO and KEGG enrichment analyses of FRDEGs, including BP, CC, MF and KEGG pathway. Horizontal coordinates are GO terms and KEGG terms. BP, CC, MF and KEGG. (B) BP enrichment analysis of FRDEGs. (C) CC enrichment analysis of FRDEGs. (D) MF enrichment analysis of FRDEGs. (E) KEGG pathway enrichment analysis of FRDEGs. Orange nodes represent entries, dark blue nodes represent molecules, and connecting lines represent the relationship between entries and molecules. The screening criteria for GO and KEGG enrichment analyses were adj. P<0.05 and FDR value (q-value) <0.25. FRDEGs, ferroptosis-related differentially expressed genes; GO, Gene Ontology; KEGG, Kyoto Encyclopedia of Genes and Genomes; BP, Biological Process; CC, Cellular Component; MF, Molecular Function.

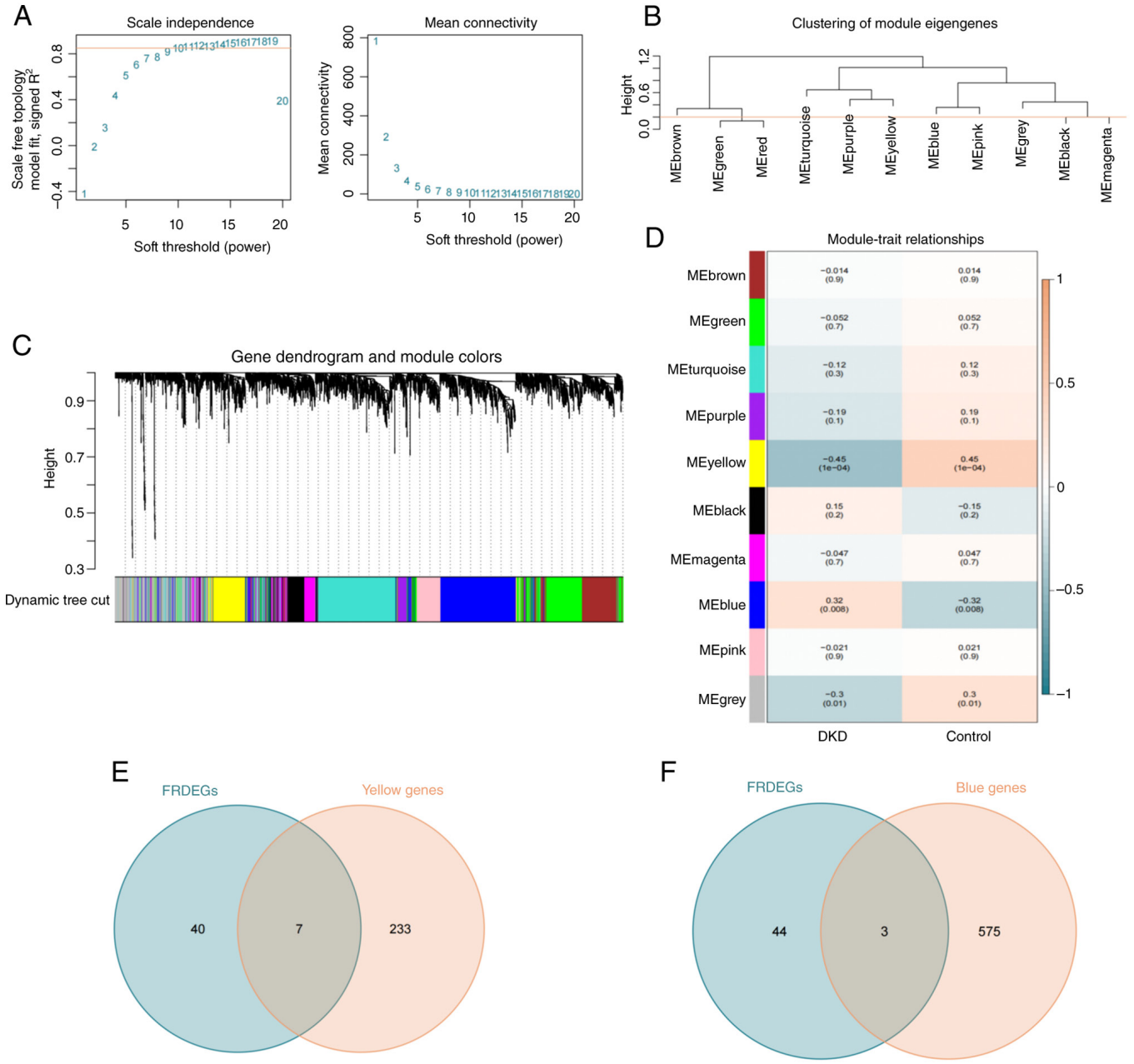

Figure 6. WGCNA for combined Gene Expression Omnibus datasets. (A) Scale-free network demonstration of the optimal soft threshold in WGCNA. The left figure shows the optimal soft threshold, and the right figure shows the network connectivity for different soft threshold cases. (B) Module aggregation results for genes in the top 25% of variance are shown. (C) Clustering results for genes with top 25% variance. The upper part shows the hierarchical clustering dendrogram and the lower part shows the gene module. (D) The results of the correlation analysis between the gene clustering module with the top 25% of variance and the DKD and control groups in the combined GEO datasets. (E and F) Venn diagram of 47 FRDEGs taking intersections with (E) MEyellow and (F) MEblue module genes, respectively. DKD, diabetic kidney disease; WGCNA, Weighted Gene Co-Expression Network Analysis; FRDEGs, ferroptosis-related differentially expressed genes.

CCL5 demonstrated significantly lower efficacy in the DKD diagnostic model than the other variables.

In order to evaluate and validate the accuracy and discriminatory capacity of the DKD diagnostic model, the role of the DKD diagnostic model was assessed in clinical utility through DCA based on ferroptosis-related hub genes in the combined GEO datasets. The results showed that the line of the DKD model was stably higher than all positive and all negative in a specific range, resulting in a substantial net gain. Consequently, the model demonstrated effectiveness in accurately diagnosing DKD (Fig. 8A). Furthermore, ROC curves were generated using the LASSO risk score derived from the combined GEO datasets (Fig. 8B). These ROC curves demonstrated the robustness of the LASSO risk score in accurately predicting the expression level within various subgroups, as evidenced by an AUC exceeding 0.9. The calculation of the LASSO risk score was performed as follows:

$$riskScore = CCL5 \times (0.3358) + FOXC1 \times (-0.3888) + LTF \times (0.8159).$$

The DKD diagnostic model's accuracy and discriminatory capacity were validated using the GSE96804 dataset.

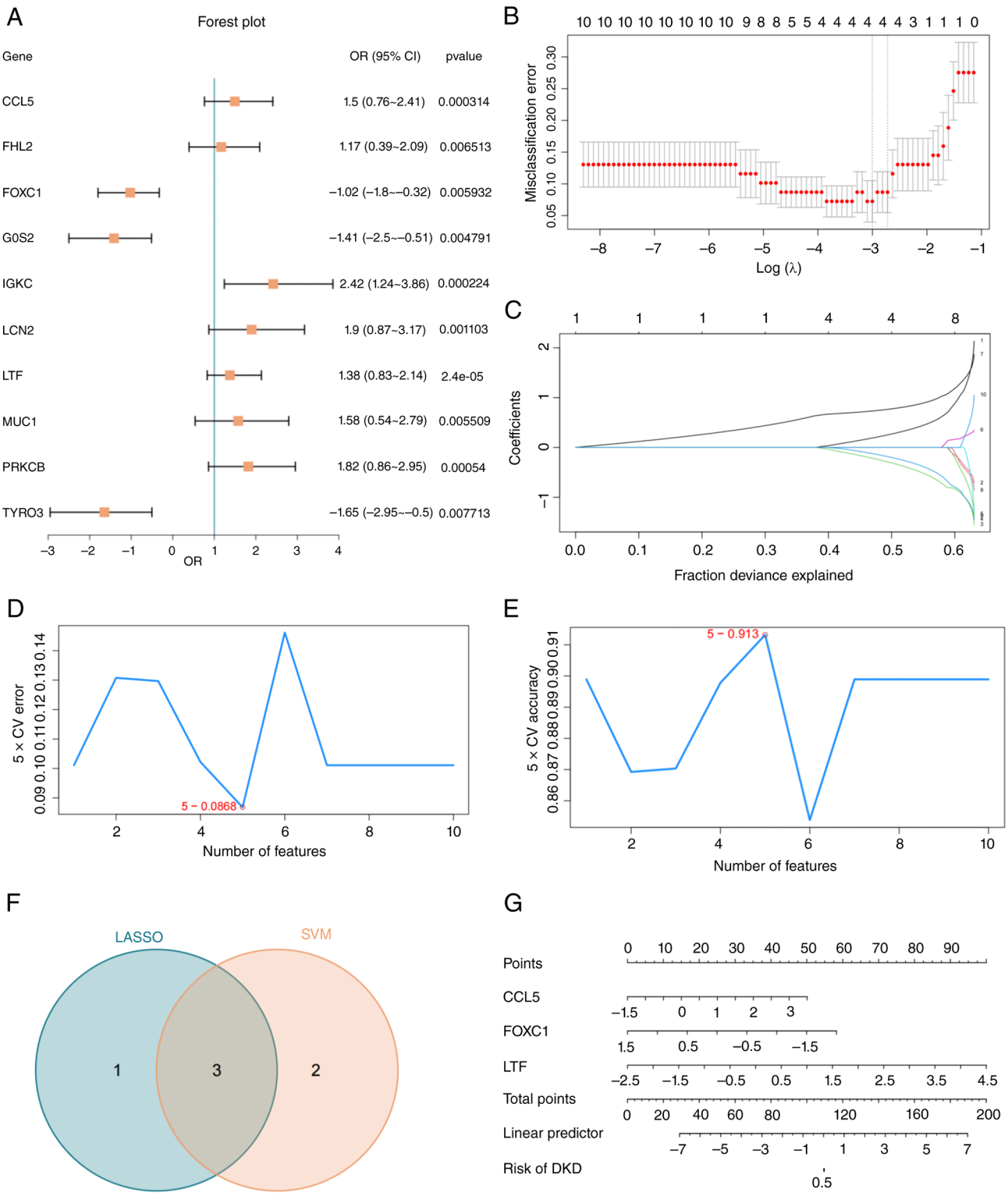

Figure 7. Diagnostic model of DKD. (A) The forest plot of the 10 key genes included in the logistic regression model in a diagnostic model for DKD. (B) Diagnostic model plot for the LASSO regression model. (C) Variable trajectory plot for the LASSO regression model. (D) Visual presentation of the number of genes with the lowest error rate obtained by the SVM algorithm. (E) Visual presentation of the number of genes with the highest accuracy obtained by the SVM algorithm. (F) Veen plots of key genes included in the LASSO regression model and the SVM model. (G) The nomogram of ferroptosis-related hub genes in a diagnostic model of DKD. DKD, diabetic kidney disease; LASSO, least absolute shrinkage and selection operator; SVM, support vector machine.

The results of the DCA demonstrated that the model consistently outperformed both the 'All positive' and 'All negative' scenarios within a specific range, indicating a high net gain and overall effectiveness (Fig. 8C). Additionally, the ROC curves revealed that the LASSO risk score expression level in the GSE96804 dataset exhibited varying accuracy across different subgroups, with AUC values ranging from 0.7 to 0.9 (Fig. 8D). Finally, a nomogram was constructed to illustrate the interplay among ferroptosis-related hub genes in dataset GSE96804 (Fig. 8E). The results showed that the expression

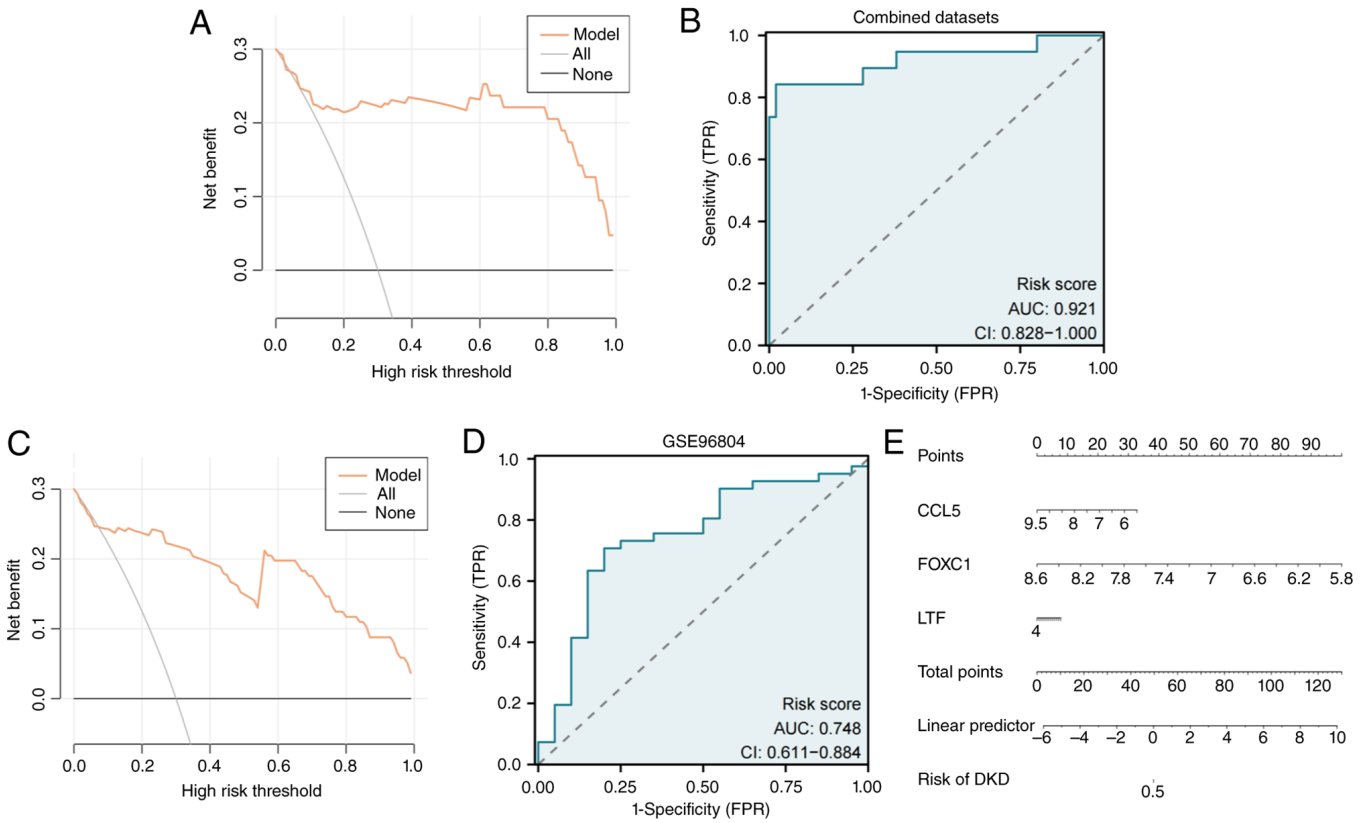

Figure 8. Diagnostic and validation analysis of DKD. (A) The DCA graph of the DKD diagnostic model based on ferroptosis-related hub genes in the combined GEO datasets. (B) The ROC curve of LASSO risk score in the combined GEO datasets. (C) The DCA graph of the DKD diagnostic model based on ferroptosis-related hub genes in the dataset GSE96804. (D) The ROC curve of LASSO risk score in the dataset GSE96804. (E) The nomogram of ferroptosis-related hub genes in the DKD diagnostic model of the dataset GSE96804. The vertical coordinate represents net gain, and the horizontal coordinate represents threshold probability. DKD, diabetic kidney disease; DCA, decision curve analysis; GEO, Gene Expression Omnibus; ROC, receiver operating characteristic; LASSO, least absolute shrinkage and selection operator; AUC, area under the curve.

of FOXC1, a ferroptosis-related hub gene, exhibited notably greater efficacy in the DKD diagnostic model compared with other variables. Conversely, the expression of LTF demonstrated significantly diminished utility in the DKD diagnostic model compared with the other variables.

Determination and validation of the optimal Hub FRDEGs. The expression of CCL5, FOXC1, and LTF were all statistically significant (P<0.05) in the DKD and control groups in the combined GEO datasets (Fig. 9A). Whereas in dataset GSE96804 (Fig. 9B), only the expression of FOXC1 and LTF were statistically significant (P<0.05). Subsequently, the accuracy of FOXC1 expression levels in the combined GEO datasets was confirmed a certain level of accuracy (0.7< AUC <0.9), as well as higher accuracy (AUC >0.9) in the GSE96804 dataset. Meanwhile, LTF in the combined GEO datasets exhibited high accuracy (AUC >0.9) in the expression levels across different groups while also demonstrating a certain level of accuracy (0.7< AUC <0.9) in the GSE96804 dataset among different subgroups (Fig. 9C-F).

CIBERSORT estimation. The CIBERSORT algorithm was employed to calculate the correlation between the 22 immune cells in the DKD group and the control group, and a histogram illustrating the percentage of immune cells in the combined GEO datasets was plotted (Fig. 10A). The box line plot (Fig. 10B) provided evidence of the disparity in immune cell infiltration abundance between DKD and control groups in the combined GEO datasets. The statistical analysis revealed that the expression levels of eight immune cell types, namely B cells naive, plasma cells, T cells gamma delta, NK cells resting, macrophages M1, macrophages M2, mast cells resting and mast cells activated, were significantly different (P<0.05) between the two groups. Subsequently, the correlation between the infiltration abundance of the eight immune cells was illustrated through correlation dot plots (Fig. 10C). The findings revealed that T cells gamma delta and macrophages M2, as well as T cells gamma delta and macrophages M1, exhibited the highest level of positive correlation (r=0.38). Conversely, mast cells resting and mast cells activated displayed the most substantial negative correlation (r=-0.45). Finally, the correlation heatmap analysis revealed that LTF and CCL5, two of the ferroptosis-related hub genes, significantly correlated with immune cells, and both showed a significant positive correlation with immune cell T cells gamma delta (Fig. 10D).

Validation of the optimal Hub FRDEGs. In the DKD group, LTF and FOXC1 exhibited higher expression levels compared with the control group, while CCL5 expression was lower. Upon intervention with RZ and HPS on the DKD model, LTF and CCL5 expression levels were significantly increased compared with the DKD group. Similarly, FOXC1 expression was significantly

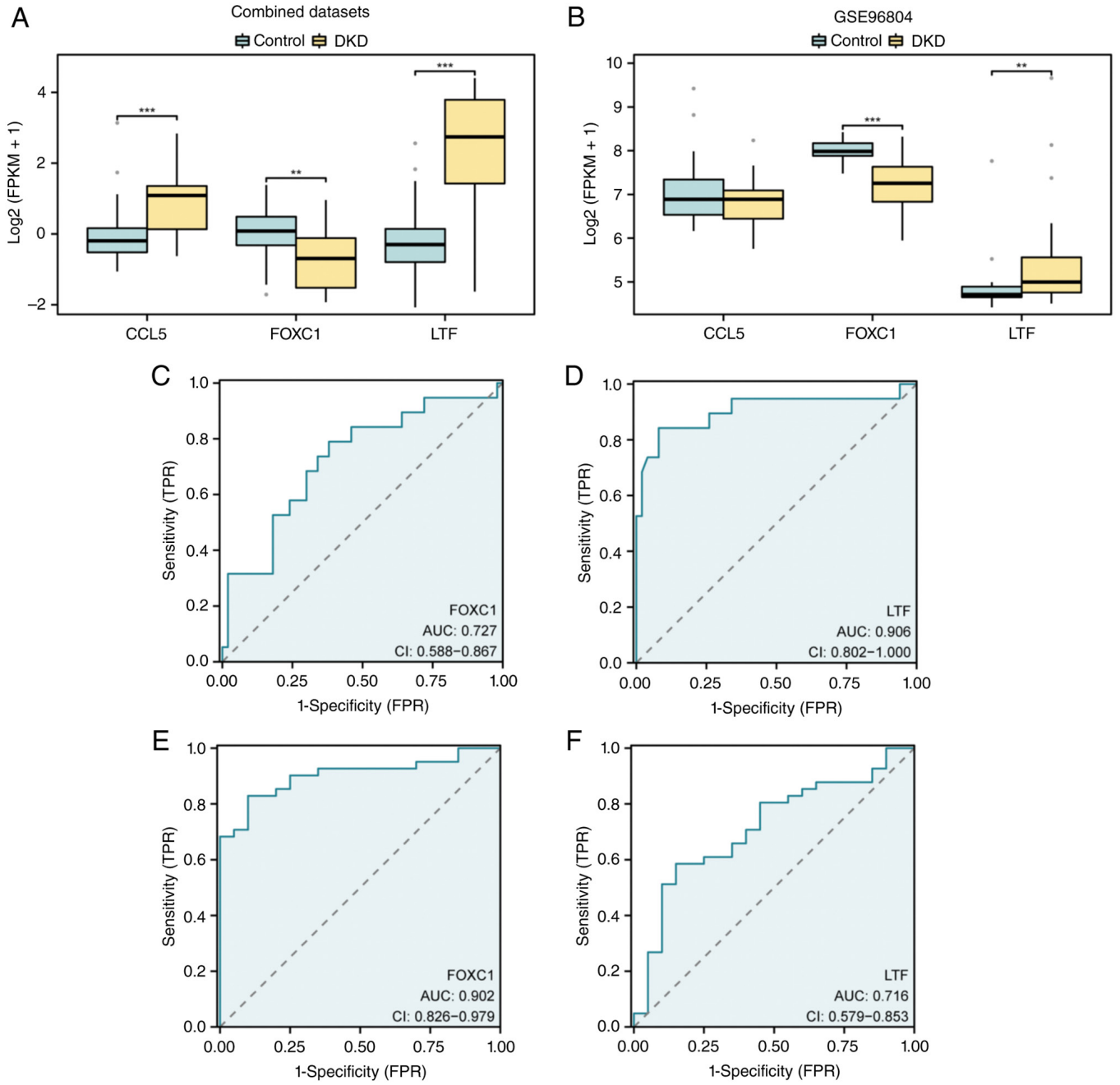

Figure 9. Expression difference analysis. (A) Boxplots of ferroptosis-related hub genes in the combined GEO datasets. (B) Boxplots of ferroptosis-related hub genes in the dataset GSE96804. (C and D) ROC curves of the two ferroptosis-related hub genes in the combined GEO datasets: (C) FOXC1and (D) LTF. (E and F) ROC curves of the two ferroptosis-related hub genes in the dataset GSE96804: (E) FOXC1and (F) LTF. The control group is blue and the DKD group is yellow. **P<0.01 and ***P<0.001. AUC 0.7-0.9 with some accuracy; above 0.9 with high accuracy. GEO, Gene Expression Omnibus; ROC, receiver operating characteristic; DKD, diabetic kidney disease; AUC, area under the curve; LTF, lactotransferrin.

elevated following interventions with HPS, although FOXC1 exhibited a trend to increase in response to RZ intervention, the difference was not statistically significant (Fig. 11).

Discussion

Ferroptosis, a regulated cell death pathway marked by the accumulation of intracellular iron overload, heightened lipid peroxidation, and an abundance of reactive oxygen species (ROS) (32), has a close association with the pathological progression of DKD. Previous studies have observed alterations in iron deposition and markers related to ferroptosis in renal tissues of different animal models of DKD (33). Furthermore, the extent of renal iron accumulation has exhibited a positive correlation with levels of serum creatinine and urinary protein (34). Iron is filtered through the glomerulus and subsequently reabsorbed in the renal tubules within the human body. These renal tubules, being energy-consuming organs, play a crucial role in reabsorbing substances against concentration gradients. To obtain the necessary energy, they rely on fatty acid oxidation, a process that takes place in numerous mitochondria (35). In the presence of elevated

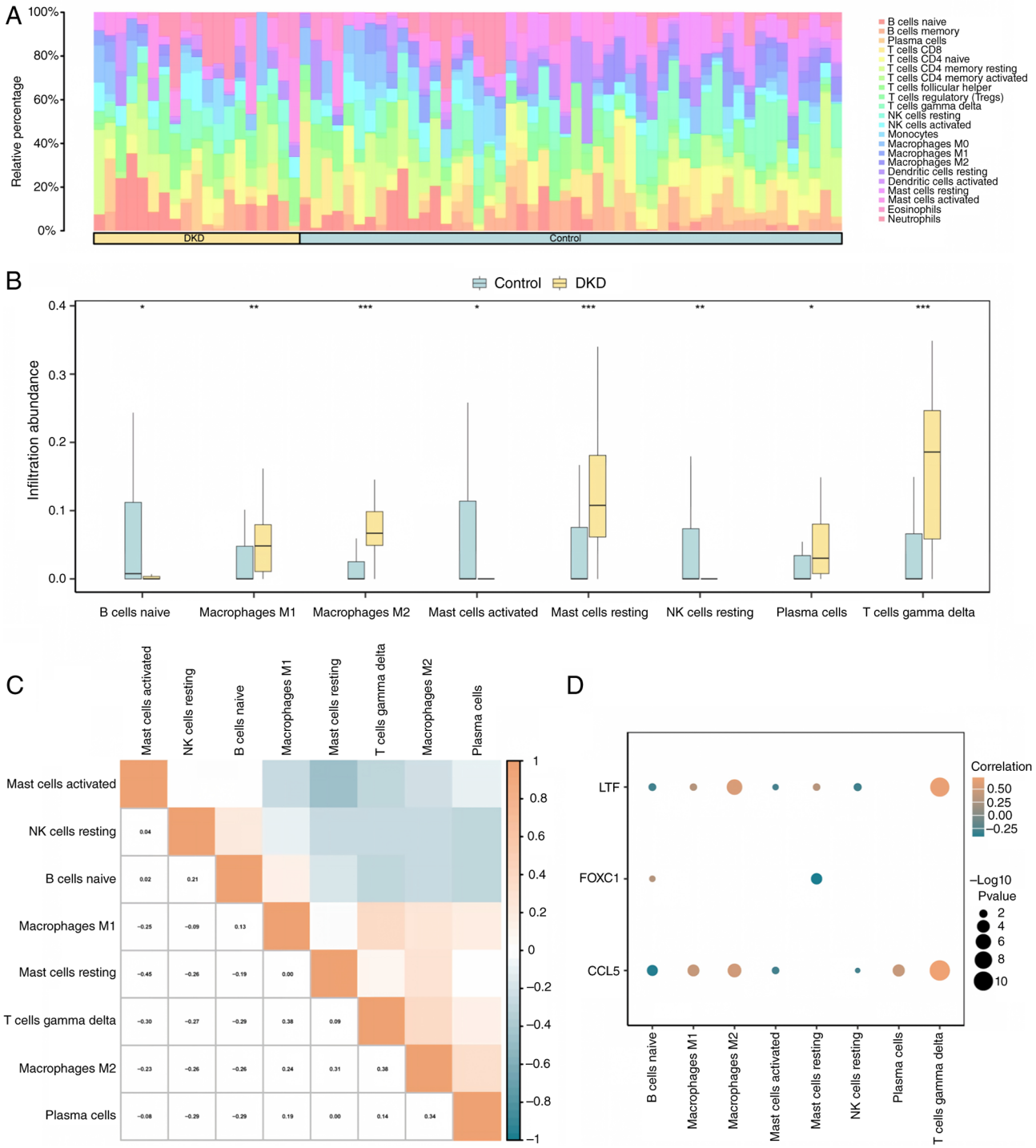

Figure 10. Combined GEO datasets immune infiltration analysis by CIBERSORT algorithm. (A) Histogram of the percentage of immune cells in the combined GEO datasets. (B) Box line plots comparing the immune cell infiltration abundance between the DKD and control groups. (C) The correlation heatmap of immune cell infiltration abundance in the combined GEO datasets. (D) The dot plot of correlation between ferroptosis-related hub genes and abundance of immune cell infiltration in the combined GEO datasets. Blue color represents the control group and yellow color represents the DKD group. Orange represents positive correlation and dark blue represents negative correlation. GEO, Gene Expression Omnibus; DKD, diabetic kidney disease.

glucose levels, renal mitochondria generate substantial quantities of ROS, leading to potential harm to various renal intrinsic cells at the genetic, transcriptional, and protein levels (36). These ROS are considered to serve as an upstream regulatory mechanism for microvascular injury induced by diabetes (37). Recent research has indicated that the inhibition of ferroptosis in renal tubular epithelial cells and the mitigation of hyperglycemia-induced decline in renal function can be achieved through the targeting of ferroptosis, such as by employing the antioxidant quercetin (38). Emerging evidence has established a definitive interplay between ferroptosis and inflammatory fibrosis in organs, and targeting ferroptosis has been proposed as a potential therapeutic strategy against renal inflammatory fibrosis. Nevertheless, further investigation is still required to fully elucidate the precise mechanisms underlying ferroptosis in DKD (39).

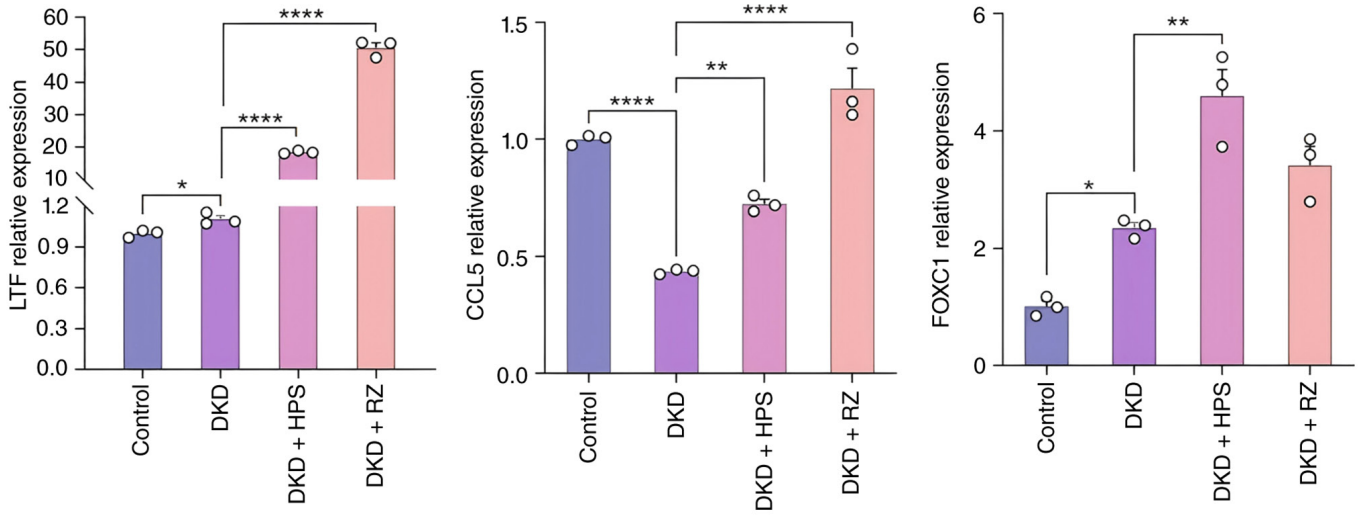

Figure 11. Validation the expression of Hub FRDEGs. Reverse transcription-quantitative PCR results for mRNA levels of LTF, CCL5 and FOXC1. Data are shown as the mean ± SD. *P<0.05, **P<0.01 and ****P<0.0001. DKD, diabetic kidney disease; RZ, rosiglitazone; HPS, hyperoside; LTF, lactotransferrin; FOXC1, forkhead box C1; CCL5, chemokine ligand 5.

The present study initially discovered that DKD was correlated with immune inflammation, apoptosis, and lipid metabolism through the utilization of GSEA and GSVA analyses. Subsequently, through the analysis of differential gene expression, a total of 47 FRGs were identified in DKD. The enrichment analysis conducted using GO and KEGG revealed a significant enrichment of FRDEGs associated with ferroptosis, hypoxia response, immune inflammation, and other functions and pathways in DKD. Among them, hypoxia-inducible factor-1 (HIF-1) is a pivotal player in the transcriptional response to oxygen homeostasis and exerts a significant influence on intracellular metabolism in the context of kidney injury (40). Extensive evidence indicates that HIF-1 orchestrates metabolic reprogramming, mitochondrial dysfunction, and the induction of inflammatory and fibrotic factors, thereby contributing to target organ damage (41). In a db/db mouse model, Feng *et al* (42) demonstrated that the HIF-1α/HO-1 pathway may mediate ferroptosis in renal tubular injury and fibrosis. Moreover, HIF-1α directly represses carnitine palmitoyl-transferase 1A promoter activity, reducing mitochondrial fatty acid transport and promoting intracellular lipid droplet formation, ultimately leading to lipotoxic stress, lipid peroxidation and ferroptosis (43,44). Additionally, leukocyte trans-endothelial migration, a key regulator of immune and inflammatory responses, may be linked to ferroptosis. In DKD, elevated glucose and lipid levels activate inflammatory signaling, leading to excessive production of pro-inflammatory factors and chemokines (10), which promote leukocyte accumulation and activation along vascular endothelial cells, initiating further inflammatory cascades (45). Chronic renal inflammation subsequently fosters a fibrotic microenvironment, driving structural remodeling and irreversible functional decline (9). Extensive research has confirmed that ferroptosis and inflammatory immune responses co-exist and mutually reinforce each other, forming a local auto-amplification loop (46). Recent studies have further validated the contribution of ferroptosis to kidney fibrosis (47,48). In DKD, damage-associated molecular patterns released by ferroptotic cells activate various immune cells, exacerbating renal damage through chemokine-or cytokine-mediated inflammatory responses (36). This process begins with the recruitment of leukocytes, predominantly neutrophils, to the site of inflammation (45). Concurrently, numerous pro-inflammatory factors and cytokines generated in DKD can stimulate immune cells, thereby inducing ferroptosis. Collectively, these findings account for the enrichment of inflammatory immune response pathways observed in our GSEA analysis.

In the present study, three ferroptosis-related hub genes (CCL5, FOXC1 and LTF) were further screened out to establish the DKD diagnostic model. CCL5, a vital member of the CC chemokine family, can recruit immune cells to sites of inflammation or injury (49) and is closely associated with DKD (50). In renal biopsy specimens from patients with DKD, CCL5 levels are notably altered, particularly in tubular cells, and correlate strongly with NF-κB activation, mesangial cell infiltration and proteinuria severity (51). Under hyperglycemic conditions, damaged tubular and mesangial cells upregulate CCL5 expression, promoting monocyte, macrophage, and T-cell recruitment into glomeruli and tubulo-interstitium, thereby exacerbating inflammation, triggering ferroptosis, and ultimately contributing to kidney injury (50). FOXC1, belonging to the FOXC subfamily of transcription factors, plays a crucial role in diverse biological processes and is indispensable for the preservation of cellular functionality and resilience against oxidative stress (52). As it is widely acknowledged, the impairment and depletion of podocytes in DKD lead to a decline in renal function (53). In this context, the regulatory role of FOXC1 in governing the expression of genes responsible for maintaining podocyte integrity is of utmost importance (54). Notably, elevated FOXC1 expression induces epithelial-mesenchymal transition (EMT) and promotes fibrosis, whereas FOXC1 suppression in high-expressing cells reverses EMT (55,56). Furthermore, high glucose conditions upregulate HIF-1α

in renal and vascular cells (57), which in turn activates FOXC1 transcription, inducing ferroptosis and causing target organ damage (58). Among the three ferroptosis-related hub genes, LTF, a glycoprotein belonging to the transferrin family, has been found to play a crucial role in the regulation of iron homeostasis (59). Several preclinical studies have demonstrated the ability of LTF to mitigate inflammation and oxidative stress, improve mitochondrial dysfunction, and act as a biomarker for ferroptosis and renal fibrosis, thereby may exerting a protective effect in DKD (60). Additionally, LTF has been shown to reduce lipid peroxidation, alleviate inflammation and oxidative stress in damaged tissues, and inhibit ferroptosis through modulation of the HGMB1/TLR-4/MyD88/Nrf2 signaling pathway (61). Mohamed *et al* (62) substantiated the role of LTF in the downregulation of ferroptosis and the safeguarding of renal tissues through by promoting NRF2/HO-1 signaling and inhibiting NF-κB pathway expression.

Therefore, *in vivo* animal experiments were further carried out to verify the role of LTF, CCL5 and FOXC1 in DKD, so as to increase the reliability of the present analysis. In addition, intervention in DKD model mice was conducted using RZ, a Western drug, and HPS, the active ingredient of the traditional Chinese medicine *Abelmoschus Manihot*, respectively; it was found that all the three ferroptosis-related hub genes were significantly elevated in both groups. Clinical studies confirmed that RZ (63,64) and *Abelmoschus Manihot* (64) can effectively treat DKD. RZ, as a drug targeting ferroptosis in the treatment of DKD, can effectively modulate the inflammatory pathway to inhibit ferroptosis, which has been demonstrated in several *in vitro* and *in vivo* studies, including those involving STZ-induced diabetic mice, db/db mice, and high glucose-treated NRK-52E and HK-2 cells (36). In 2020, Wang *et al* (5) verified that RZ could reduce urinary albumin levels by inhibiting ferroptosis and inflammation in db/db mice. The present study suggested that RZ significantly affected the ferroptosis-related biomarkers in DKD, which might contribute to subsequent studies exploring the mechanisms and targets of RZ in the treatment of DKD. Meanwhile, HPS, a flavonoid compound, is established as the exclusive quality control indicator for *Abelmoschus Manihot* in the 2020 edition of the Chinese Pharmacopoeia and represents the principal active constituent in *Abelmoschus manihot* (65). It predominantly localizes in the kidneys and livers of animals (66). HPS demonstrates anti-inflammatory, antioxidant and immunomodulatory activities. Extensive research has substantiated its efficacy in alleviating DKD, with evidence indicating its therapeutic benefits through the improvement of ferroptosis (66,67). LTF, CCL5 and FOXC1, the target ferroptosis-related hub genes, may be essential targets for HPS in treating DKD, thereby providing ideas for future research.

Imbalances in human immune function are inextricably linked to the development of DKD (9). Infiltration of immune cells in renal tissues is a distinctive feature of DKD, associated with an increased risk of DKD progression (50). Immune cell infiltration analysis revealed dysregulation in eight distinct immune cell types between patients with DKD and the controls. Specifically, γδT cells, M1 macrophages, M2 macrophages and resting mast cells exhibited significantly higher levels in renal tissues of patients with DKD than the controls. Moreover, there existed distinct regulatory associations among these different immune cells. γδT cells are unconventional T cells with unique T cell receptors on their surface. Despite comprising 1-5% of T cells in peripheral blood, γδT cells possess remarkable potency and versatility. They serve as a crucial link between innate and adaptive immunity, playing multiple roles in inflammation regulation, tissue repair and damage surveillance (68). Renal tissues afflicted with tubulointerstitial fibrosis exhibited considerably elevated γδ T cell counts compared with healthy renal tissues (69). Additionally, these γδ T cells were found to generate substantial quantities of the pro-inflammatory cytokine IL-17A, thereby facilitating the renal inflammatory response (68,69). In the presence of elevated glucose levels, a significant influx of macrophages occurs within the kidney and secrete diverse pro-inflammatory mediators (70). This process induces renal inflammation and fibrosis, thereby expediting renal injury and playing a pivotal role in the progression of DKD, aligning with prior research findings (70,71). In an inflammatory environment, γδ T cells can regulate macrophages through direct interactions, cytokine secretion and chemotaxis induction, leading to macrophage proliferation, activation, and polarization towards either pro-inflammatory (M1-like) or anti-inflammatory (M2-like) states (72,73). It is consistent with the significant positive correlation between γδ T cells and macrophages observed in the present study.

Significantly, the present study revealed a notable positive correlation between the FRGs LTF and CCL5 and γδT cells, suggesting their involvement in the immune microenvironment of DKD. From a functional perspective, this correlation is biologically plausible. Activated human γδT cells have been shown to express functional lactoferrin receptors at a markedly higher proportion than αβT cells, making them particularly responsive to LTF-mediated immunoregulation. LTF may suppress ferroptosis through the NRF2/HO-1 and NF-κB pathways (57,58), while also modulating γδT cell activity via iron-dependent mechanisms. Regarding CCL5, emerging evidence indicates that γδT cell-derived IL-17A can promote renal fibrosis through CCL5-mediated leukocyte infiltration (66,74), establishing a functional link between γδT cells and CCL5-driven chemotaxis. Therefore, the interplay between γδT cells and these hub genes suggests a complex immuno-regulatory network in which γδT cells contribute to both the inflammatory milieu and ferroptosis-associated pathology in DKD. LTF, a crucial factor in facilitating both innate and acquired immune responses (74), exhibited a considerably higher proportion of expression in activated γ-δ T cells compared with activated α-β T cells (75). Meanwhile, it has been observed that CCL5, a chemokine, plays a significant role in facilitating the recruitment of T-cells to both glomeruli and tubular interstitium (50). In conclusion, the observed strong association between ferroptosis and the infiltration of immune cells implied that ferroptosis could potentially play a role in the pathogenesis of DKD by triggering immune cell infiltration and subsequent immune responses. Further investigation is warranted to validate these bioinformatic predictions through overexpression or knockout models of the identified hub genes.

There are inevitable limitations to our study that should be acknowledged. Firstly, one notable obstacle encountered

was the lack of renal specimens from patients with DKD, which consequently necessitated the future conduction of a prospective clinical study to validate the clinical applicability of the present model. Secondly, the validation in the present study was confined to RT-qPCR analysis of CCL5, LTF and FOXC1, with no protein-level verification or further mechanistic investigation into immune-inflammatory pathways and ferroptosis. Further studies are required to corroborate these findings at the protein level and to elucidate the precise mechanisms through which FRGs and immune cell infiltration contribute to DKD. In future basic DKD experiments, it is intended to validate all the pertinent ferroptosis markers *in vivo* and *in vitro* and explore the immune-inflammatory pathways that may be regulated by the target hub genes, thereby enhancing the persuasiveness of the present analysis. Last but not least, the observed discrepancy regarding FOXC1 expression levels and analytical outcomes may be attributed to the limited sample size and inherent biological heterogeneity. It is noteworthy that the bioinformatic analysis was conducted using publicly available human renal specimens, whereas experimental validation was performed in the mouse kidney model, introducing potential interspecies variations. Furthermore, RNA expression is inherently subject to temporal and spatial specificity. Although FOXC1 is expressed across multiple renal cell types, including podocytes, vascular endothelial cells and tubular epithelial cells, its regulatory mechanisms may vary in a cell type-dependent manner. Differences in cellular composition or DKD staging between the bioinformatic cohorts and the experimental model may also contribute to the divergent results. Therefore, further validation using a substantial number of human renal tissues from both DKD patients and control subjects is essential to corroborate the diagnostic biomarkers more comprehensively. Additionally, leveraging single-nucleus RNA sequencing could help elucidate the cell type-specific expression profiles of FOXC1 in DKD. Nevertheless, the present study provides a basis for exploring ferroptosis mechanisms in DKD and targets for future therapies.

In the present study, a total of 47 FRDEGs were screened. Through bioinformatics analysis, three hub genes (CCL5, LTF and FOXC1) were identified, which are closely associated with the development of DKD. These findings contribute to the enhanced comprehension of the molecular pathological mechanisms underlying DKD, offering potential benefits in terms of diagnosis and therapeutic interventions targeting ferroptosis and immune cell infiltration. However, additional experimental investigations are warranted to validate the role of ferroptosis in DKD.

Acknowledgements

Not applicable.

Funding

The present study was supported by the National Natural Science Foundation of China (grant nos. 82374355 and 82575019), the Science and Technology Support Program of Jiangsu (grant no. ZT202206), the Jiangsu Traditional Chinese Medicine Science and Technology Development Plan Project (grant no. QN202506) and the Jiangsu Hospital of Chinese Medicine Institutional Research Projects (grant no. Y25066).

Availability of data and materials

The data generated in the present study may be requested from the corresponding author.

Authors' contributions

YT conceptualized and supervised the study, visualized, curated and validated data, conduced formal analysis and project administration, developed methodology, performed software analysis, wrote the original draft, and wrote, reviewed and edited the manuscript. ZL curated data, performed formal analysis and wrote the original draft. SS conducted formal analysis and developed methodology. LZ performed formal analysis and supervised the study. YS contributed to data organization and statistical analysis. XZ contributed to the study design and experimental validation. JY and QY conceptualized and supervised the study, acquired funding, validated data, conducted project administration, and wrote, reviewed and edited the manuscript. YT and QY confirm the authenticity of all the raw data. All authors read and approved the final version of the manuscript.

Ethics approval and consent to participate

Animal experiments received the approval from the Animal Ethics Committee in Affiliated Hospital of Nanjing University of Traditional Chinese Medicine (approval no. 2023DW-039-01; Nanjing, China) and were conducted in accordance with institutional and national guidelines for the care and use of laboratory animals.

Patient consent for publication

Not applicable.

Competing interests

The authors declare that they have no competing interests.

References

1. Afkarian M, Zelnick LR, Hall YN, Heagerty PJ, Tuttle K, Weiss NS and de Boer IH: Clinical manifestations of kidney disease among US adults with diabetes, 1988-2014. JAMA 316: 602-610, 2016.
2. Zhang L, Long J, Jiang W, Shi Y, He X, Zhou Z, Li Y, Yeung RO, Wang J, Matsushita K, *et al*: Trends in chronic kidney disease in China. N Engl J Med 375: 905-906, 2016.
3. Zheng J and Conrad M: The metabolic underpinnings of ferroptosis. Cell Metab 32: 920-937, 2020.
4. Jiang X, Stockwell BR and Conrad M: Ferroptosis: Mechanisms, biology and role in disease. Nat Rev Mol Cell Biol 22: 266-682, 2021.
5. Wang Y, Bi R, Quan F, Cao Q, Lin Y, Yue C, Cui X, Yang H, Gao X and Zhang D: Ferroptosis involves in renal tubular cell death in diabetic nephropathy. Eur J Pharmacol 888: 173574, 2020.
6. Sanz AB, Sanchez-Niño MD, Ramos AM and Ortiz A: Regulated cell death pathways in kidney disease. Nat Rev Nephrol 19: 281-299, 2023.

7. Ilyas Z, Chaiban JT and Krikorian A: Novel insights into the pathophysiology and clinical aspects of diabetic nephropathy. Rev Endocr Metab Disord 18: 21-28, 2017.
8. Anders HJ, Huber TB, Isermann B and Schiffer M: CKD in diabetes: Diabetic kidney disease versus nondiabetic kidney disease. Nat Rev Nephrol 14: 361-377, 2018.
9. Tang SCW and Yiu WH: Innate immunity in diabetic kidney disease. Nat Rev Nephrol 16: 206-222, 2020.
10. Rayego-Mateos S, Rodrigues-Diez RR, Fernandez-Fernandez B, Mora-Fernández C, Marchant V, Donate-Correa J, Navarro-González JF, Ortiz A and Ruiz-Ortega M: Targeting inflammation to treat diabetic kidney disease: The road to 2030. Kidney Int 103: 282-296, 2023.
11. Woroniecka KI, Park AS, Mohtat D, Thomas DB, Pullman JM and Susztak K: Transcriptome analysis of human diabetic kidney disease. Diabetes 60: 2354-2369, 2011.
12. Na J, Sweetwyne MT, Park ASD, Susztak K and Cagan RL: Diet-induced podocyte dysfunction in Drosophila and mammals. Cell Rep 12: 636-647, 2015.
13. Pan Y, Jiang S, Hou Q, Qiu D, Shi J, Wang L, Chen Z, Zhang M, Duan A, Qin W, *et al*: Dissection of glomerular transcriptional profile in patients with diabetic nephropathy: SRGAP2a protects podocyte structure and function. Diabetes 67: 717-730, 2018.
14. Shi JS, Qiu DD, Le WB, Wang H, Li S, Lu YH and Jiang S: Identification of transcription regulatory relationships in diabetic nephropathy. Chin Med J (Engl) 131: 2886-2890, 2018.
15. Davis S and Meltzer PS: GEOquery: A bridge between the gene expression omnibus (GEO) and BioConductor. Bioinformatics 23: 1846-1847, 2007.
16. Leek JT, Johnson WE, Parker HS, Jaffe AE and Storey JD: The sva package for removing batch effects and other unwanted variation in high-throughput experiments. Bioinformatics 28: 882-883, 2012.
17. Ritchie ME, Phipson B, Wu D, Hu Y, Law CW, Shi W and Smyth GK: Limma powers differential expression analyses for RNA-sequencing and microarray studies. Nucleic Acids Res 43: e47, 2015.
18. Stelzer G, Rosen N, Plaschkes I, Zimmerman S, Twik M, Fishilevich S, Stein TI, Nudel R, Lieder I, Mazor Y, *et al*: The GeneCards suite: From gene data mining to disease genome sequence analyses. Curr Protoc Bioinformatics 54: 1.30.1-1.30.33, 2016.
19. Liang JY, Wang DS, Lin HC, Chen XX, Yang H, Zheng Y and Li YH: A novel ferroptosis-related gene signature for overall survival prediction in patients with hepatocellular carcinoma. Int J Biol Sci 16: 2430-2441, 2020.
20. Subramanian A, Tamayo P, Mootha VK, Mukherjee S, Ebert BL, Gillette MA, Paulovich A, Pomeroy SL, Golub TR, Lander ES and Mesirov JP: Gene set enrichment analysis: A knowledge-based approach for interpreting genome-wide expression profiles. Proc Natl Acad Sci USA 102: 15545-15550, 2005.
21. Hänzelmann S, Castelo R and Guinney J: GSVA: Gene set variation analysis for microarray and RNA-seq data. BMC Bioinformatics 14: 7, 2013.
22. Liberzon A, Subramanian A, Pinchback R, Thorvaldsdottir H, Tamayo P and Mesirov JP: Molecular signatures database (MSigDB) 3.0. Bioinformatics 27: 1739-1740, 2011.
23. Mi H, Muruganujan A, Ebert D, Huang X and Thomas PD: PANTHER version 14: More genomes, a new PANTHER GO-slim and improvements in enrichment analysis tools. Nucleic Acids Res 47 (D1): D419-D426, 2019.
24. Kanehisa M and Goto S: KEGG: Kyoto encyclopedia of genes and genomes. Nucleic Acids Res 28: 27-30, 2000.
25. Yu G, Wang LG, Han Y and He QY: clusterProfiler: An R package for comparing biological themes among gene clusters. OMICS 16: 284-287, 2012.
26. Langfelder P and Horvath S: WGCNA: An R package for weighted correlation network analysis. BMC Bioinformatics 9: 559, 2008.
27. Engebretsen S and Bohlin J: Statistical predictions with glmnet. Clin Epigenetics 11: 123, 2019.
28. Sanz H, Valim C, Vegas E, Oller JM and Reverter F: SVM-RFE: Selection and visualization of the most relevant features through non-linear kernels. BMC Bioinformatics 19: 432, 2018.
29. Van Calster B, Wynants L, Verbeek JFM, Verbakel JY, Christodoulou E, Vickers AJ, Roobol MJ and Steyerberg EW: Reporting and interpreting decision curve analysis: A guide for investigators. Eur Urol 74: 796-804, 2018.
30. Newman AM, Liu CL, Green MR, Gentles AJ, Feng W, Xu Y, Hoang CD, Diehn M and Alizadeh AA: Robust enumeration of cell subsets from tissue expression profiles. Nat Methods 12: 453-457, 2015.
31. Livak KJ and Schmittgen TD: Analysis of relative gene expression data using real-time quantitative PCR and the 2(-Delta Delta C(T)) method. Methods 25: 402-408, 2001.
32. Li J, Cao F, Yin HL, Huang ZJ, Lin ZT, Mao N, Sun B and Wang G: Ferroptosis: past, present and future. Cell Death Dis 11: 88, 2020.
33. Dominguez JH, Liu Y and Kelly KJ: Renal iron overload in rats with diabetic nephropathy. Physiol Rep 3: e12654, 2015.
34. Chaudhary K, Chilakala A, Ananth S, Mandala A, Veeranan-Karmegam R, Powell FL, Ganapathy V and Gnana-Prakasam JP: Renal iron accelerates the progression of diabetic nephropathy in the HFE gene knockout mouse model of iron overload. Am J Physiol Renal Physiol 317: F512-F517, 2019.
35. Ma J, Li C, Liu T, Zhang L, Wen X, Liu X and Fan W: Identification of markers for diagnosis and treatment of diabetic kidney disease based on the ferroptosis and immune. Oxid Med Cell Longev 2022: 9957172, 2022.
36. Wang H, Liu D, Zheng B, Yang Y, Qiao Y, Li S, Pan S, Liu Y, Feng Q and Liu Z: Emerging role of ferroptosis in diabetic kidney disease: Molecular mechanisms and therapeutic opportunities. Int J Biol Sci 19: 2678-2694, 2023.
37. Yuchen C, Hejia Z, Fanke M, Qixin D, Liyang C, Xi G, Yanxia C, Xiongyi Y, Zhuohang X, Guoguo Y and Min F: Exploring the shared molecular mechanism of microvascular and macrovascular complications in diabetes: Seeking the hub of circulatory system injury. Front Endocrinol (Lausanne) 14: 1032015, 2023.
38. Feng Q, Yang Y, Qiao Y, Zheng Y, Yu X, Liu F, Wang H, Zheng B, Pan S, Ren K, *et al*: Quercetin ameliorates diabetic kidney injury by inhibiting ferroptosis via activating Nrf2/HO-1 signaling pathway. Am J Chin Med 51: 997-1018, 2023.
39. Lai W, Wang B, Huang R, Zhang C, Fu P and Ma L: Ferroptosis in organ fibrosis: From mechanisms to therapeutic medicines. J Transl Int Med 12: 22-34, 2024.
40. Tang D, Chen X, Kang R and Kroemer G: Ferroptosis: Molecular mechanisms and health implications. Cell Res 31: 107-125, 2021.
41. Chen Y, Zhang J, Zhang M, Song Y, Zhang Y, Fan S, Ren S, Fu L, Zhang N, Hui H and Shen X: Baicalein resensitizes tamoxifen-resistant breast cancer cells by reducing aerobic glycolysis and reversing mitochondrial dysfunction via inhibition of hypoxia-inducible factor-1α. Clin Transl Med 11: e577, 2021.
42. Feng X, Wang S, Sun Z, Dong H, Yu H, Huang M and Gao X: Ferroptosis enhanced diabetic renal tubular injury via HIF-1α/HO-1 pathway in db/db mice. Front Endocrinol (Lausanne) 12: 626390, 2021.
43. Du W, Zhang L, Brett-Morris A, Aguila B, Kerner J, Hoppel CL, Puchowicz M, Serra D, Herrero L, Rini BI, *et al*: HIF drives lipid deposition and cancer in ccRCC via repression of fatty acid metabolism. Nat Commun 8: 1769, 2017.
44. Helsley RN, Park SH, Vekaria HJ, Sullivan PG, Conroy LR, Sun RC, Romero MDM, Herrero L, Bons J, King CD, *et al*: Ketohexokinase-C regulates global protein acetylation to decrease carnitine palmitoyltransferase 1a-mediated fatty acid oxidation. J Hepatol 79: 25-42, 2023.
45. Maas SL, Soehnlein O and Viola JR: Organ-specific mechanisms of transendothelial neutrophil migration in the lung, liver, kidney, and aorta. Front Immunol 9: 2739, 2018.
46. Linkermann A, Stockwell BR, Krautwald S and Anders HJ: Regulated cell death and inflammation: An auto-amplification loop causes organ failure. Nat Rev Immunol 14: 759-767, 2014.
47. Lai W, Huang R, Wang B, Shi M, Guo F, Li L, Ren Q, Tao S, Fu P and Ma L: Novel aspect of neprilysin in kidney fibrosis via ACSL4-mediated ferroptosis of tubular epithelial cells. MedComm (2020) 4: e330, 2023.
48. Wang B, Yang LN, Yang LT, Liang Y, Guo F, Fu P and Ma L: Fisetin ameliorates fibrotic kidney disease in mice via inhibiting ACSL4-mediated tubular ferroptosis. Acta Pharmacol Sin 45: 150-165, 2024.
49. Qiu Y, Tang J, Zhao Q, Jiang Y, Liu YN and Liu WJ: From diabetic nephropathy to end-stage renal disease: The effect of chemokines on the immune system. J Diabetes Res 2023: 3931043, 2023.
50. Cao H, Rao X, Jia J, Yan T and Li D: Exploring the pathogenesis of diabetic kidney disease by microarray data analysis. Front Pharmacol 13: 932205, 2022.
51. Mezzano S, Aros C, Droguett A, Burgos ME, Ardiles L, Flores C, Schneider H, Ruiz-Ortega M and Egido J: NF-kappaB activation and overexpression of regulated genes in human diabetic nephropathy. Nephrol Dial Transplant 19: 2505-2512, 2004.
52. Lay K, Kume T and Fuchs E: FOXC1 maintains the hair follicle stem cell niche and governs stem cell quiescence to preserve long-term tissue-regenerating potential. Proc Natl Acad Sci USA 113: E1506-E1515, 2016.

53. Yin T, Yang L, Tang L, Li J, Liu D, Guo F, Mu Y, Wu Q, Feng Y, Tan Z, *et al*: Podocyte FFAR4 deficiency aggravated glomerular diseases and aging. Mol Ther 33: 4636-4654, 2025.
54. Motojima M, Kume T and Matsusaka T: Foxc1 and Foxc2 are necessary to maintain glomerular podocytes. Exp Cell Res 352: 265-272, 2017.
55. Gilding LN and Somervaille TCP: The diverse consequences of FOXC1 deregulation in cancer. Cancers (Basel) 11: 184, 2019.
56. Li Q, Wu J, Wei P, Xu Y, Zhuo C, Wang Y, Li D and Cai S: Overexpression of forkhead Box C2 promotes tumor metastasis and indicates poor prognosis in colon cancer via regulating epithelial-mesenchymal transition. Am J Cancer Res 5: 2022-2034, 2015.
57. Iacobini C, Vitale M, Pugliese G and Menini S: Normalizing HIF-1α signaling improves cellular glucose metabolism and blocks the pathological pathways of hyperglycemic damage. Biomedicines 9: 1139, 2021.
58. Lin YJ, Shyu WC, Chang CW, Wang CC, Wu CP, Lee HT, Chen LJ and Hsieh CH: Tumor hypoxia regulates forkhead box C1 to promote lung cancer progression. Theranostics 7: 1177-1191, 2017.
59. Madkour AH, Helal MG, Said E and Salem HA: Dose-dependent renoprotective impact of lactoferrin against glycerol-induced rhabdomyolysis and acute kidney injury. Life Sci 302: 120646, 2022.
60. Zahan MS, Ahmed KA, Moni A, Sinopoli A, Ha H and Uddin MJ: Kidney protective potential of lactoferrin: Pharmacological insights and therapeutic advances. Korean J Physiol Pharmacol 26: 1-13, 2022.
61. Essam RM, Saadawy MA, Gamal M, Abdelsalam RM and El-Sahar AE: Lactoferrin averts neurological and behavioral impairments of thioacetamide-induced hepatic encephalopathy in rats via modulating HGMB1/TLR-4/MyD88/Nrf2 pathway. Neuropharmacology 236: 109575, 2023.
62. Mohamed OS, Abdel Baky NA, Sayed-Ahmed MM, Al-Najjar AH. Lactoferrin alleviates cyclophosphamide induced-nephropathy through suppressing the orchestration between Wnt4/β-catenin and ERK1/2/NF-ϰB signaling and modulating klotho and Nrf2/HO-1 pathway. Life Sci. 2023;319:121528.
63. Miyazaki Y, Cersosimo E, Triplitt C and DeFronzo RA: Rosiglitazone decreases albuminuria in type 2 diabetic patients. Kidney Int 72: 1367-1373, 2007.
64. Bjornstad P, Hughan K, Kelsey MM, Shah AS, Lynch J, Nehus E, Mitsnefes M, Jenkins T, Xu P, Xie C, *et al*: Effect of surgical versus medical therapy on diabetic kidney disease over 5 years in severely obese adolescents with type 2 diabetes. Diabetes Care 43: 187-195, 2020.
65. Chen YZ, Gong ZX, Cai GY, Gao Q, Chen XM, Tang L, Wei RB and Zhou JH: Efficacy and safety of flos *Abelmoschus manihot* (Malvaceae) on type 2 diabetic nephropathy: A systematic review. Chin J Integr Med 21: 464-472, 2015.
66. Luan F, Wu Q, Yang Y, Lv H, Liu D, Gan Z and Zeng N: Traditional uses, chemical constituents, biological properties, clinical settings, and toxicities of *Abelmoschus manihot* L.: A comprehensive review. Front Pharmacol 11: 1068, 2020.
67. Xu S, Chen S, Xia W, Sui H and Fu X: Hyperoside: A review of its structure, synthesis, pharmacology, pharmacokinetics and toxicity. Molecules 27: 3009, 2022.
68. Zhang K, Li M, Yin K, Wang M, Dong Q, Miao Z, Guan Y, Wu Q and Zhou Y: Hyperoside mediates protection from diabetes kidney disease by regulating ROS-ERK signaling pathway and pyroptosis. Phytother Res 37: 5871-5882, 2023.
69. Kaminski H, Couzi L and Eberl M: Unconventional T cells and kidney disease. Nat Rev Nephrol 17: 795-813, 2021.
70. Law BMP, Wilkinson R, Wang X, Kildey K, Lindner M, Beagley K, Healy H and Kassianos AJ: Effector γδ T cells in human renal fibrosis and chronic kidney disease. Nephrol Dial Transplant 34: 40-48, 2019.
71. Calle P and Hotter G: Macrophage phenotype and fibrosis in diabetic nephropathy. Int J Mol Sci 21: 2806, 2020.
72. Yan J, Li X, Liu N, He JC and Zhong Y: Relationship between macrophages and tissue microenvironments in diabetic kidneys. Biomedicines 11: 1889, 2023.
73. Vigeland CL, Collins SL, Chan-Li Y, Hughes AH, Oh MH, Powell JD and Horton MR: Deletion of mTORC1 activity in CD4+ T cells is associated with lung fibrosis and increased γδ T cells. PLoS One 11: e0163288, 2016.
74. Hu W, Zhang X, Sheng H, Liu Z, Chen Y, Huang Y, He W and Luo G: The mutual regulation between γδ T cells and macrophages during wound healing. J Leukoc Biol 115: 840-851, 2024.
75. Actor JK, Hwang SA and Kruzel ML: Lactoferrin as a natural immune modulator. Curr Pharm Des 15: 1956-1973, 2009.
76. Mincheva-Nilsson L, Hammarström S and Hammarström ML: Activated human gamma delta T lymphocytes express functional lactoferrin receptors. Scand J Immunol 46: 609-618, 1997.